A STUDY OF ORBITS IN TWO-WAY SCALING FFAG SYNCHROTRONS

M. J. PENTZ and N. VOGT-NILSEN
CERN, Geneva, Switzerland
(presented by N. Vogt-Nilsen)

I. INTRODUCTION

The following paper is mainly intended to present computational results pertaining to linear and nonlinear orbits in two-way scaling FFAG Synchrotrons. The study was initiated by the desire to investigate the possibilities of designing at CERN a two-way model for electrons in the region of 100 Mev final energy. The results are, however, presented in scaled units, and are therefore, by proper choice of scale, relevant to particles of any charge, mass and energy.

Similar investigations have been carried out at other accelerator centers. In particular the MURA group in Madison, Wisc. has investigated the same problem in great detail with relation to their two-way 40 Mev electron model.[1]

Under the provision that the machines under investigation shall be equally able to accommodate particles going round the machine in both directions along geometrically identical orbits, this two-way feature requires the existence of an axial plane of azimuthal antisymmetry for the magnetic guide field.[2] Consequently, only radial-sector field configurations come into consideration. Furthermore, primarily for reasons of keeping the two betatron-oscillation frequencies under control, in order to avoid the multitude of nonlinear resonances, but also for reasons of mathematical simplicity, we have restricted the present study to cover only so-called scaling structures.[3] For these the two betatron frequencies are left rigorously constant throughout the acceleration process.

From the point of view of an rf acceleration by means of radially positioned accelerating cavities, it must be considered desirable, in order to avoid an unnecessarily excessive excitation of radial betatron oscillations by the cavity gap fields, that the family of equilibrium orbits in the machine cross the gaps perpendicularly. To achieve this simultaneously for both directions of rotation, there must exist axial planes of symmetry at which the gaps must be placed. Furthermore, if the positioning of rf cavities requires the existence of straight sections, these will presumably have the least effect, on betatron frequencies and nonlinear stability limits, when placed at a point of symmetry in the field. Accordingly, all fields investigated have axial planes of symmetry in addition to the planes of antisymmetry mentioned above. In the cases of straight sections, these are invariably to be placed at the planes of symmetry. Finally, the existence of symmetry planes permits the use of greatly simplifying methods of calculation.

The general radial-sector scaling accelerator field is defined, in polar coordinates, on the median plane by the axial component,

$$B_z(r,\theta) = B_0(r/r_0)^k f(\theta), \qquad (1)$$

where $f(\theta)$ defines the azimuthal flutter (involving the features of antisymmetry and symmetry), and the constant parameter k is the so-called field index. B_0 and r_0 are constants, B_0 being the field at radius r_0 at an azimuth θ for which $f(\theta)$ equals unity.

Magnet model studies performed at CERN,[4] seem to indicate that the type of flutter, for which the scaling requirement and the design tolerances are most easily met, is of purely sinusoidal shape. For this reason the majority of fields investigated have $f(\theta) = \sin M\theta$, M being the number of magnet periods of the machine. However, the effect of small amounts of higher order harmonics is also studied, as well as the introduction of a small number of hard-edged radial field-free straight sections of varying length.

During the study a number of digital computer programmes have been designed. All computational methods and programmes are described in detail in a previous report.[5] Most of these were finally compiled into a multipurpose programme by means of which one may perform any of the various types of calculation necessary in connection with an FFAG radial-sector scaling accelerator study. The basic equations and relations used in the programmes may be found in the appendix of ref. (4) or in ref. (5). For further information on the results of the present study, the reader is referred to a more extensive and detailed CERN report which will appear shortly under the same title as that of the present paper.

II. COMPUTATIONAL METHODS

The orbital equations governing the motion of charged particles in the field (1) become independent of the field constants B_0 and r_0 and of the particle mass, charge and energy, when expressed in terms of the scaled variables

$$\rho = r/S, \qquad \zeta = z/S \tag{2}$$

with a scale factor

$$S = r_0 \left(\frac{p}{qB_0 r_0}\right)^{\frac{1}{k+1}} \tag{3}$$

r,z being the conventional cylindrical coordinates, q the charge of the particle and p its momentum. Using the azimuthal angle θ as independent variable, the scaled equations of motion are then derivable from the Hamiltonian

$$H = \mp \rho[1 - (p_\rho - U_1)^2 - p_\zeta^2]^{1/2}. \tag{4}$$

Here the double sign corresponds to a motion in the positive or negative angular direction respectively, p_ρ, p_ζ denote the canonical conjugate momenta to ρ, ζ, and

$$U_1 = \rho^{k+1} \sum_{j=1}^{\infty} \sum_{\alpha=1}^{j} C_{j,\alpha} \frac{d^{2\alpha-1} f(\theta)}{d\theta^{2\alpha-1}} \left(\frac{\zeta}{\rho}\right)^{2j} \tag{5}$$

The coefficients $C_{j,\alpha}$, dependent only on the field index, may be derived from the recursion formulas:

$$C_{1,1} = -\frac{1}{2} \quad C_{2,1} = \frac{k^2}{24} C_{2,2} = \frac{1}{24}$$

$$C_{j,1} = -\frac{(k+4-2j)^2}{2j(2j-1)} C_{j-1,1}$$

$$C_{j,\alpha} = -\frac{(k+4-2j)^2 C_{j-1,\alpha} + C_{j-1,\alpha-1}}{2j(2j-1)} \tag{6}$$

$$(\alpha = 2, 3, \cdots, j-1)$$

$$C_{j,j} = \frac{(-1)^j}{(2j)!} \quad (j = 3, 4, 5, \cdots)$$

On the median plane the Hamiltonian reduces to

$$H_m = \mp \rho(1 - p_\rho^2)^{1/2} + \frac{f(\theta)}{k+2} \rho^{k+2} \tag{7}$$

The closed equilibrium orbit for an M-sector machine is described by the periodic solution governed by this Hamiltonian. The scaled equilibrium orbit will be correct for a particle of momentum

$$p = qB_0 r_0^{-k} \tag{8}$$

whereafter any other orbit may be found by linear scaling with the factor (3).

The simplest and most economical manner used to determine the equilibrium orbit is based on the assumed existence of symmetry and antisymmetry in the field flutter. Due to these, there will exist points of symmetry in the flutter function $f(\theta)$ spaced by one-half magnet period. These points of symmetry are reflected in the geometry of the equilibrium orbit, which may be defined as the median-plane orbit for which the canonical momentum p_ρ vanishes at the points of field symmetry. During computation, a succession of orbits starting with $p_\rho = 0$ at a point of flutter symmetry is automatically computed through one half field period such that, by a method of interpolation, each new orbit is chosen closer to the required one defined by $p_\rho = 0$, also at the final half-period point. This method gives a rapid convergence towards the equilibrium orbit. The process is stopped when a given accuracy, usually six figures, is attained.

The programme may equally be set to determine, by the same method, higher order, closed, median-plane orbits; i.e., orbits which are periodic with some multiple n of the field

period $2\pi/M$. Thus an nth-order closed orbit may be found by using the same method through $n/2$ magnet periods.

Having successfully determined the equilibrium orbit, the digital computer automatically sets about finding the two linearized betatron-oscillation frequencies Q_R, Q_Z. This is accomplished by solving the two pairs of linear equations

$$\begin{aligned} x' &= \pm \frac{p_{\rho 0}}{\psi_0} x \pm \frac{\rho_0}{\psi_0^3} p_x \\ p_x' &= -(k+1) f \rho_0^k x \mp \frac{p_{\rho 0}}{\psi_0} p_x \\ \zeta' &= \pm \frac{\rho_0}{\psi_0} p_\zeta \\ p_\zeta' &= \rho_0^k \left(kf \mp \frac{p_{\rho 0}}{\psi_0} f' \right) \zeta \\ \psi_0 &= (1 - p_{\rho 0}^2)^{1/2} \end{aligned} \tag{9}$$

where ρ_0, $p_{\rho 0}$ denote the equilibrium orbit and x, p_x the relative coordinates $\rho - \rho_0$, $p_\rho - p_{\rho 0}$ respectively. The equations (9) are derived by introducing these new coordinates in the Hamiltonian (4), expanding this in a power series in x, p_x, ζ, p_ζ and retaining only the terms of second order. From these equations, the two linear transfer matrices T_R, T_Z for the two modes of oscillation through one magnet period are determined, whereafter the frequencies are given in units of oscillations per period by

$$\cos\left(Q_j \frac{2\pi}{M}\right) = 1/2 \text{ trace } T_j, \ (j = R, Z) \tag{10}$$

The significance of the two Q-values, as basic design parameters, reaches further than that of the linearized betatron oscillations alone. As is well known,[6] the working point (Q_R, Q_Z) must not be chosen too close to the set of dangerous higher-order intrinsic or error-induced resonance lines for the coupled nonlinear betatron oscillations defined by certain linear relations between the Q's.

An arbitrary median-plane orbit will behave in a very complex manner when followed around the machine. This is due partly to the scallop of the equilibrium orbit to which it belongs, and partly to the nonlinear radial betatron oscillations about this orbit. For a general off-median-plane orbit, matters are further complicated by the axial oscillations and the coupling between the two modes of motion. As is well known, the major part of the orbit complexity is suppressed by displaying the phase points as they occur, successively, at azimuthal positions spaced by one magnet field period. Viewed stroboscopically in this manner, only the pure betatron oscillations are left for observation. Thus in a ρ, p_ρ phase plane, the equilibrium orbit is displayed as a fixed point, and nth-order closed median-plane orbits as a set of n periodic points, or nth-order fixed points.

Experience with digital computers seems to show that each set of higher-order fixed points lies on a corresponding set of invariant curves, or separatrices. For stable radial motion, these separatrices are closed curves whereas, for unstable motion, they tend towards the point at infinity. This definition for stability is used for median-plane motion throughout this report.

One must assume that, for the more complicated off-median plane coupled motion, there also exist invariants, but as these are now embedded in a 4-dimensional phase space they are impossible to detect by the simple means of plotting. Accordingly, a more crude definition is used for the 4-dimensional motion; viz., that an orbit is stable if it successfully traverses a preset number of magnet periods (usually 250). The stability boundaries obtained in this manner are surprisingly sharp, provided that the number of magnet periods used is not chosen too low.

III. FIELD WITH SINUSOIDAL FLUTTER FUNCTIONS

A. Extent of the Investigation

As mentioned in the introduction, the fields most intensively studied are those having a purely sinusoidal flutter function $f(\theta) = \sin(M\theta)$. The field is thus defined by only two basic parameters; viz., the period number M and the field index k. All phase-space plots presented pertain to the point of symmetry $\theta = 2\pi/M$ at maximum field.

The computations have been carried out for values of k between 5 and 15, and M values between 13 to 22, as indicated by the encircled points in Fig. 1. The radial stability limits

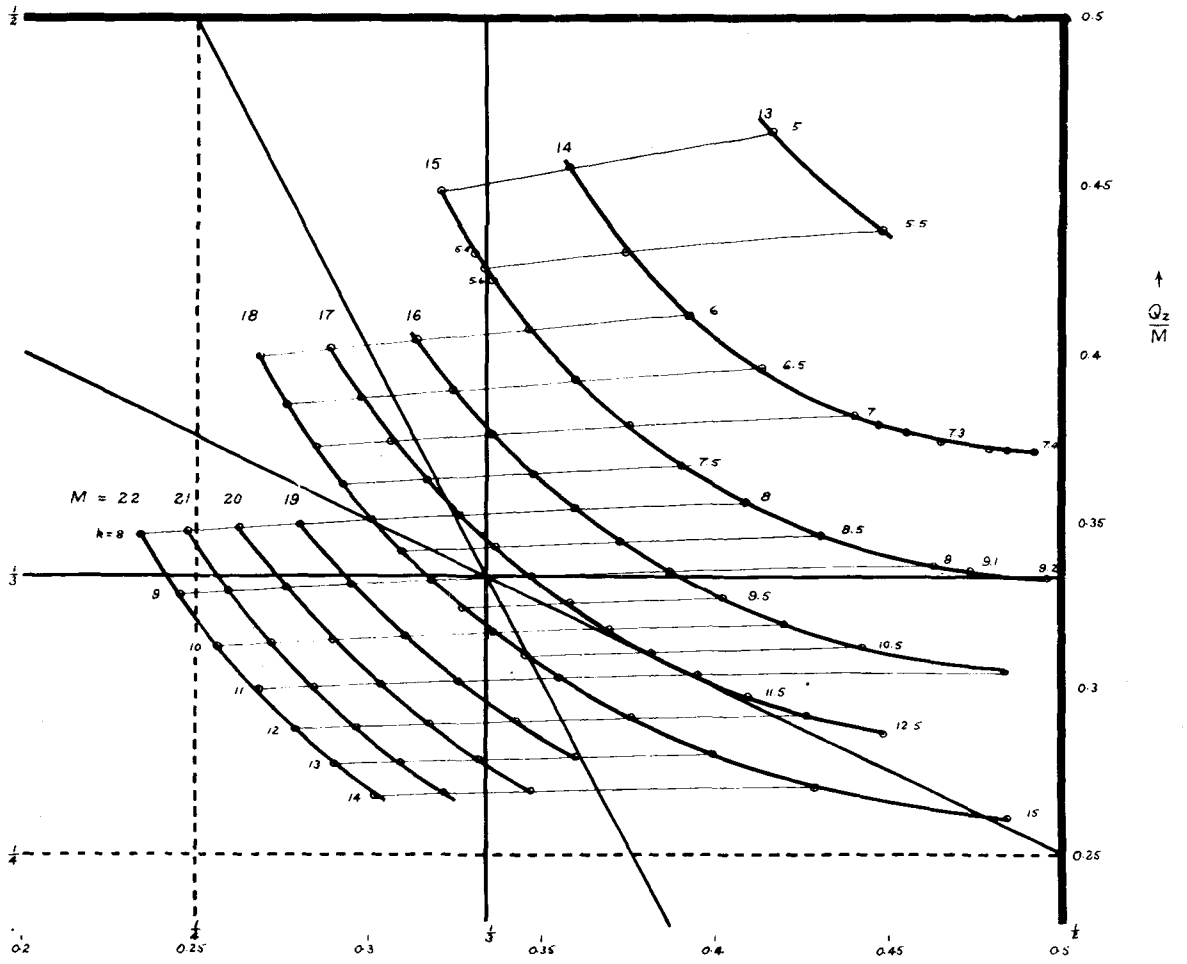

Fig. 1 Linear betatron oscillation frequencies for sinusoidal flutters.

have been determined for the majority of these cases, whereas the vertical limits, for reasons of time economy, only for a limited subset of cases.

B. Linearized Oscillations

For all values of k and M studied, both the radial and vertical betatron-oscillation frequencies Q_R/M and Q_Z/M, measured in betatron oscillations per magnet period, lie in the interval 0.2 to 0.5. Their variation with k for each value of M is shown on Fig. 1. On the figure are also shown the intrinsic resonance lines $Q/M=\frac{1}{2}$, $\frac{1}{3}$, $\frac{1}{4}$ and $2Q_Z/M+Q_R/M=1$; $Q_Z/M+2Q_R/M=1$, of which the latter and $Q_Z/M=\frac{1}{3}$ are excited only by imperfections in the median-plane geometry.

One is, of course, interested in choosing an operating point (k,M) such as to give the largest possible *nonlinear* radial and vertical stability limits. In this case, higher-order resonances than the ones shown in Fig. 1 are of importance, as is shown in the next section. Since the betatron frequencies will, in general, decrease with increasing amplitude of oscillation about the equilibrium orbit (though in certain cases the betatron frequency increases initially), and since the lower-order resonances are the most dangerous, it would be expected that the operating points which lie the furthest above $Q/M=\frac{1}{3}$ or $Q/M=\frac{1}{4}$ (provided that, if they are below the $\frac{1}{3}$ resonance, they are not so near to it as to become unstable while Q is *increasing* with amplitude) would give the largest stability limits. This is borne out, approximately, by the results reported in the next section.

For certain purposes it is of interest to have an operating point at which $Q_R = Q_Z$, for instance, where it is intended to deal with radiation anti-damping by coupling the vertical and radial oscillations.

It is found that the relation between k and M subject to this condition is very nearly linear and may be expressed by the empirical formula

$$k \approx 0.80M - 5.0. \qquad (11)$$

In view of the practical difficulty of making an FFAG magnet for which k is constant over the radial aperture, it is of interest to choose a value of M for which the sensitivity of Q to k is as low as possible. It is evident from Fig. 1 that this sensitivity tends to decrease with increasing M. From the practical point of view, however, it becomes increasingly difficult to construct a magnet of a given size with a flutter function independent of radius as M is increased. Consequently, a realistic figure of merit for the k-sensitivity would be the quantity $Mk(\Delta Q/\Delta k)$ which is plotted in Fig. 2. The curves indicate a preference for values of M between 16 and 18.

C. Nonlinear Radial Stability Limits

In this section the median plane orbits, as computed from the Hamiltonian (7), are investigated for the sinusoidal fields under consideration. All the orbits studied start at the point of field maximum with the canonical momentum $p_\rho = 0$. Thus the orbits are distinguished by only one further parameter, viz., the initial scaled radius ρ.

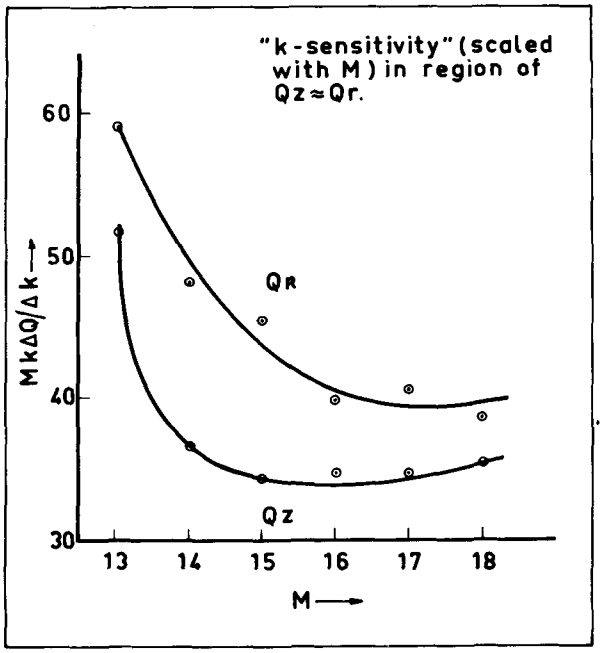

Fig. 2 "k-sensitivity" (scaled with M) in region $Q_Z \approx Q_R$.

To determine the radial stability limit or limiting separatrix on the ρ, p_ρ phase plane, we have used the digital computer to find the existing fixed points of increasing order, and studied their limiting separatrices. For topological reasons, the limiting separatrices must be of one of the forms indicated, for example, by a set of third-order limiting fixed points in Fig. 3. The separatrix cross-over points on the diagrams are the unstable fixed points, while the circles represent stable fixed points. On each diagram, the positive sense of the ρ-axis may be inverted. With a stroboscopic view at a point of field symmetry, as exclusively used in this connection, all diagrams will be symmetric about the ρ-axis. Hence, for odd-order limiting

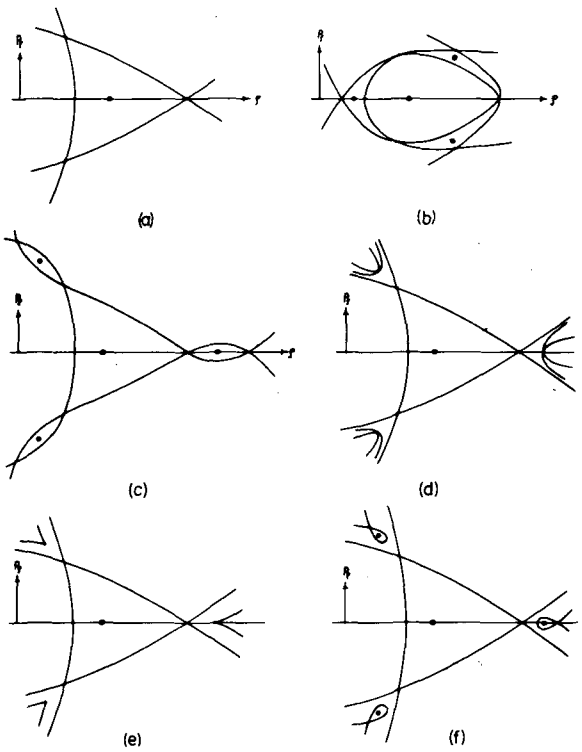

Fig. 3 Topology of third-order limiting separatrices
a. Simple separatrix
b. Separatrix with edge islands
c. Separatrix with corner islands
d. } Separatrix with unstable external fixed points
e. }
f. Separatrix with external islands

separatrices there will always exist unstable fixed points on the ρ-axis, which is what our computer programme is capable of finding. This may not be so for even-order cases.

In such cases, a stroboscopic view one-half magnet period ahead will again yield unstable fixed points with $p_\rho = 0$. As is readily inferred from Fig. 3, each type of topology may be distinguished by the number of locally stable and unstable fixed points on the ρ-axis and their positions mutual, and relative, to the known first-order equilibrium-orbit fixed point. That one really has determined the limiting separatrix is tested by starting an orbit slightly outside the unstable $p_\rho = 0$ fixed point. Such an orbit will rapidly find itself in a region where the magnetic field is sufficiently strong to reverse the azimuthal sense of rotation in the accelerator. This is registered by the digital computer, and the orbit counted as unstable.

The search for radial-stability limits, by this fixed point method, is considerably facilitated by the use of a table of rational fractions in the range 0.2 to 0.5 of interest in the present study. As an illustration, the linear Q_R/M in a particular case ($M = 14$, $k = 7.4$) has the value 0.4789. With increasing amplitude, fixed points of order 15, 37, 31, 20, etc., corresponding to the decreasing rational fractions,

7/15 = 0.4666	17/40 = 0.4250
17/37 = 0.4595	13/33 = 0.4242
14/31 = 0.4516	11/26 = 0.4231
9/20 = 0.4500	8/19 = 0.4210
4/9 = 0.4444	13/31 = 0.4194
3/7 = 0.4286	5/12 = 0.4167

were searched for and determined. Of these, the 7th-order points (rational fraction = 3/7) were identified as lying on the limiting separatrix by the methods outlined previously.

In a number of cases, for all of which the linear Q_R/M lies somewhat below 1/3, the nonlinear Q_R/M is found to increase initially, moving, that is, towards 1/3, and then to decrease, giving a double set of internal fixed points of the same order within the limiting separatrix. In such cases it is the presence of the 1/3 resonance that determines the motion at smaller amplitudes, while the 1/4 resonance dominates the motion at larger amplitudes.

The variation of the radial betatron-oscillation frequency with amplitude is shown for some representative cases in Figs. 4 and 5.

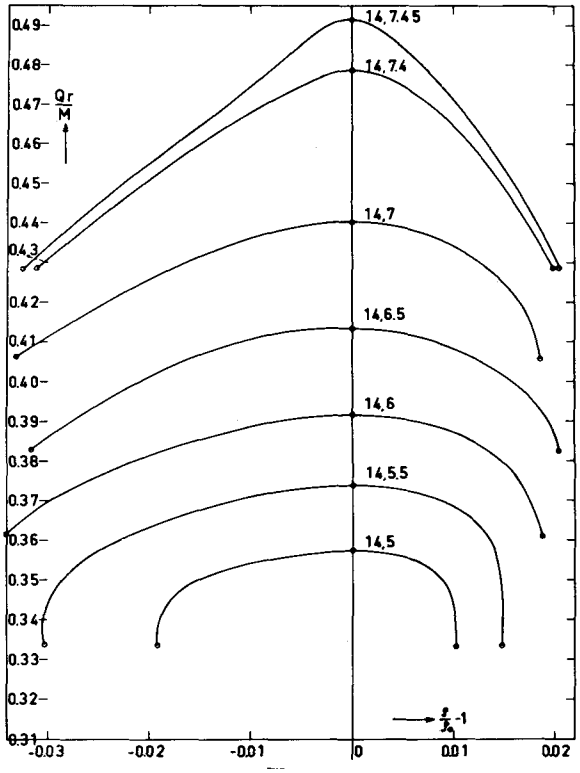

Fig. 4 Fixed point curves for $M = 14$.

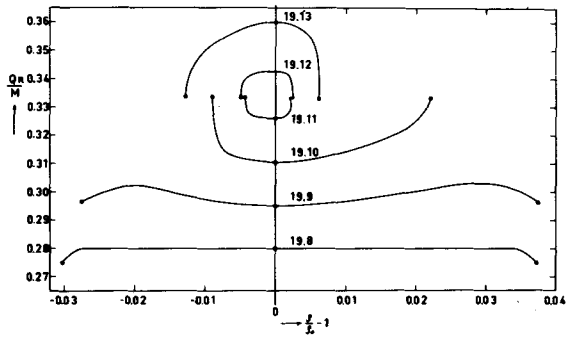

Fig. 5 Fixed point curves for $M = 19$.

Here the value of Q_R/M appropriate to each higher-order fixed point on the ρ-axis is plotted as a function of the normalized radial displacement $(\rho/\rho_0 - 1)$, ρ being the radius at which the fixed point is located and ρ_0 the equilibrium-orbit radius. The two parameters attached to each curve are (M, k). The case (19, 9) in Fig. 5 is an example of the previously mentioned double-fixed-point set in the region between the 1/3 and 1/4 resonances. A corresponding phenomenon has been found for $M = 22$ in the region between the 1/4 and 1/5 resonances. For these

cases, the radial Q is nearly constant out to very large amplitudes, and the radial stability limits are found to be exceptionally large.

To indicate the magnitude of the region of radial stability, we have used the quantity

$$S_R = 100\Delta\rho/\rho_0, \tag{12}$$

$\Delta\rho$ being the radial extent along the ρ-axis of the stable region viewed stroboscopically at a point of field maximum symmetry. In Fig. 6, S_R is plotted for various values of M as a function of the linear (zero-amplitude) Q_R/M. The curves probably have a finer structure than is apparent with the limited number of points available, with subsidiary minima at resonances of order higher than 4. The sharp destructive resonance at $\frac{1}{3}$ and the less sharp one at $\frac{1}{4}$ are clearly shown, however, as are the regions below $\frac{1}{3}$ and $\frac{1}{4}$ where the radial limits are exceptionally wide.

Fig. 7 shows an example of a ρ, p_ρ phase plot ($M=18$, $k=7$, $Q_R/M=0.2885$, $S_R=7.03$ percent). Here the limiting separatrix is of 7th order of the edge island type (Fig. 3b).

It should perhaps be mentioned that evidence, due to other investigators in this field, seems to indicate that, for working-points in the neighborhood of resonances involving Q_Z, an infinitesimally small initial axial motion might cause instability. Hence, in such regions of the Q-diagram the results given here might be taken with some reserve. For the cases studied here (see sections 3D, 4C and 5), no such anomalies have been detected.

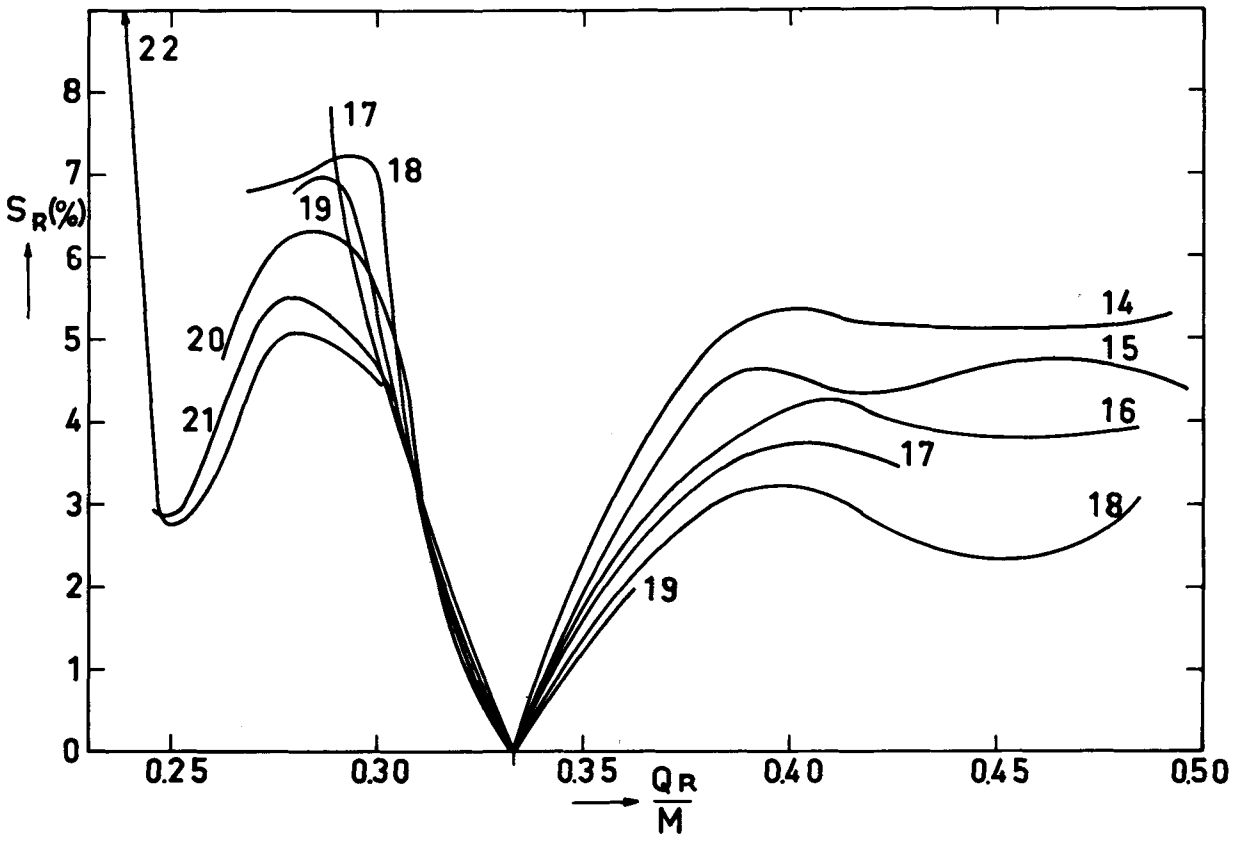

Fig. 6 Radial stability limits for sinusoidal flutters.

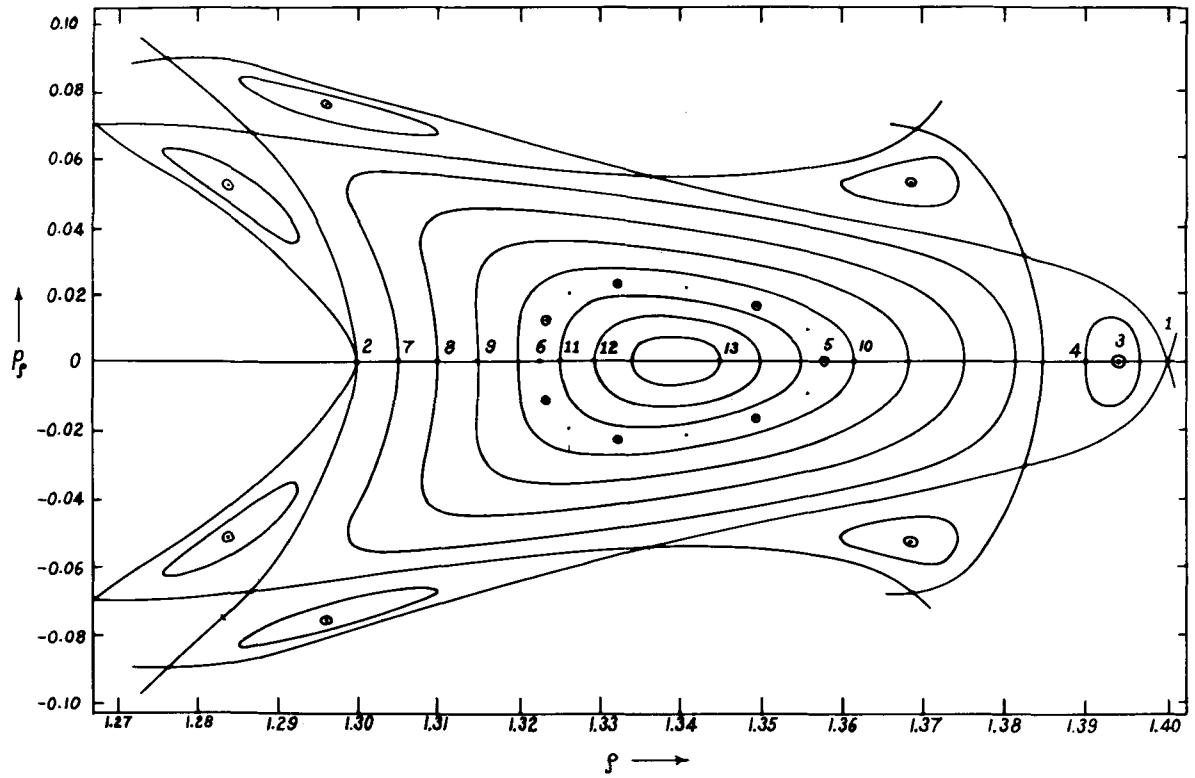

Fig. 7 7th order limiting separatrix ($M=18$, $k=7$).
1,2 : 7th order separatrix fixed points
3 : 7th order island fixed points
4 : 7th order islands
5,6 : 7th order internal fixed points
7-13: Quasi-linear internal trajectories

D. Nonlinear Axial Stability Limits

In order to determine the stability limits for the coupled 4-dimensional motion, the more crude method was used of systematically running-off orbits, with stepwise decreasing betatron-oscillation amplitudes, until one finally finds one which survives a large prechosen number of periods (usually 250). By repeating the method with smaller and smaller steps, a sharp stability limit could be found.

The geometrical significance of the two canonical momenta, p_ρ and p_ζ, is that of representing the angular and axial slope of the orbit under consideration. If one remembers that the orbits are invariably viewed at a point of field symmetry where the equilibrium orbit slopes vanish, it is clear that the canonical momenta will be fairly small in any actual design. For reasons of simplicity and digital-computer-time economy, the dependence of the axial-stability limits on small values of the two initial canonical momenta has only been checked in a few cases, and then found to have no significant influence on the results. Thus, for the present exploratory study, it has been considered sufficient to set the initial momenta at the field maximum to zero, and introduce only one additional parameter for the digital computer runs, namely, the initial scaled axial coordinate ζ. The computed orbits, therefore, differ only in the four parameters: M, k and the initial ρ, ζ.

The results may be illustrated graphically by the representative example shown for $M=15$ in Fig. 8. For each value of the field index k, a series of ζ-limit searches, as outlined above, have been performed at a set of values of the initial ρ within the radially stable region. The resulting limits are indicated by the encircled

points on the figure. The area beneath the curve, drawn through these points and the extreme points for radial-stable motion, together with the symmetric image of this area with respect to the ρ-axis, then represents with fair accuracy the ρ, ζ-section of the phase space available for stable coupled oscillations.

Corresponding to the quantity (12), defining the magnitude of the median-plane stable region, we introduce here the number

$$S_Z = 200\zeta_{\mathrm{lim}}/\rho_0 \qquad (13)$$

to indicate the degree of axial stability. ζ_{lim} is then the height of the curves in Fig. 8 measured directly above the equilibrium-orbit scaled radius ρ_0; ζ_{lim} does not, in general, coincide with the maxima of the curves in Fig. 8.

Table 1 gives the quantity S_Z for the fields investigated for axial oscillations.

TABLE 1

Sinusoidal Fields

M	k	Q_R/M	Q_Z/M	S_R	S_Z
13	5.00	0.4157	0.4657	6.24	1.8
14	5.50	0.3738	0.4305	4.44	4.2
	6.50	0.4131	0.3957	5.22	5.0
	7.40	0.4789	0.3719	5.13	4.4
15	5.00	0.3206	0.4486	2.14	2.8
	6.00	0.3458	0.4076	1.49	4.0
	7.10	0.3771	0.3763	3.91	6.2
	7.50	0.3902	0.3668	4.65	4.6
	8.25	0.4188	0.3509	4.56	4.6
	8.50	0.4305	0.3461	4.41	4.4
16	6.00	0.3135	0.4044	3.20	5.4
	7.86	0.3560	0.3569	2.14	2.6
	8.00	0.3595	0.3538	2.51	2.2
	10.00	0.4200	0.3191	4.10	2.2
17	8.00	0.3265	0.3520	0.82	2.0
	9.00	0.3470	0.3335	1.31	0.6
18	8.00	0.3009	0.3504	6.79	0.3
22	12.00	0.2791	0.2875	5.10	3.6

If one compares these results with the positions of the corresponding working points in Fig. 1, it is seen that, generally speaking, the axial extent of the stable region is of the same magnitude as the radial extent, and fairly large, for points well away from any resonance lines. For points in the proximity of these lines, one notices a corresponding reduction in the extent of the stability region.

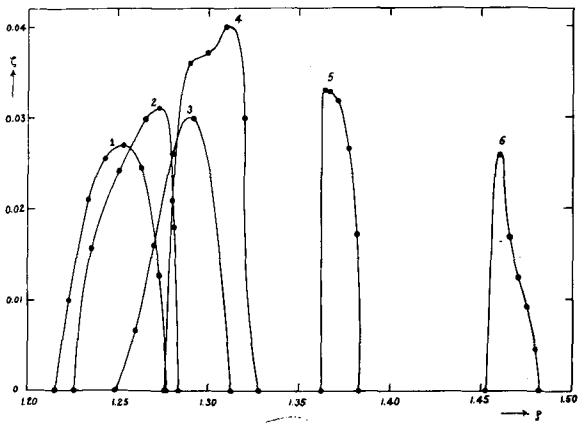

Fig. 8 Axial stability limits for sinusoidal flutters ($M=15$):
1. $k=8.5$
2. $k=8.25$
3. $k=7.5$
4. $k=7.1$
5. $k=6.0$
6. $k=5.0$

IV. INTRODUCTION OF STRAIGHT SECTIONS IN SINUSOIDAL FIELDS

A. Sinusoidal Flutters with Superperiods

In the design of a radial-sector FFAG accelerator, a problem of some importance is the insertion of a number of straight sections for the accelerating cavities.

In the case of a symmetrical (two-way) accelerator, it is necessary to preserve the condition that there shall exist at least one plane of antisymmetry at some azimuthal position. This imposes a restriction on the number of pole pairs, N, for a given number of gaps, n. If the n gaps are to be located at planes of symmetry, which is necessary if the orbits are to cross the gaps normally, there must also be n planes of anti-symmetry. It then follows that the number of magnet poles between symmetry planes must be odd, i.e., $2N/n=2j+1$, $j=0, 1, 2, \ldots$ Consequently, the allowable values of N and n are as shown in Table 2.

TABLE 2

No. of gaps n	Allowable no. of magnet pole pairs N				
2	1	3	5	7	9
4	2	6	10	*14*	*18*
6	3	19	*15*	21	27

The values of N chosen for the present study were 14, 15, and 18, with the corresponding values of $n=4$, 6 and 4. In the first and last cases, there are two superperiods around the magnet, and in the second case there are three. They are, therefore, designated $M=2(14)$, $M=3(15)$ and $M=2(18)$, respectively, the first number denoting the number of true magnet periods—or superperiods.

For the purpose of a preliminary study of the effects of straight sections of various lengths, an idealized field configuration was chosen, which has the form shown in Fig. 9. The azimuthal length of one magnet pole is called Y, and the azimuthal length of the straight section X. The flutter function is sinusoidal except at the straight sections, where it drops discontinuously to zero. This configuration is designated "hard-edge, zero-field, straight section." Some computations have been made on modified forms of this configuration, which will be described in subsection E.

B. Linearized Oscillations

Owing to the effects of integral and half-integral resonances of the superperiod structure, the radial and axial linear betatron-oscillation frequencies Q_R/N and Q_Z/N are confined to narrower limits than was the case with sinusoidal fields without superperiods. Their variation with k and with the ratio X/Y is shown in Figs. 10–12 for the three structures $M=2(18)$, 2(14) and 3(15) respectively. Each curve is labelled with the appropriate value of X/Y, and the relevant integral and half-integral superperiod resonance lines are shown.

The three sets of curves show certain similarities and certain much more striking dissimilarities. The similarities are confined to the

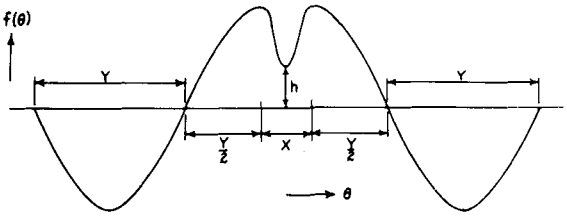

Fig. 9 Hard-edge zero-field straight section.

variation of Q_Z with k, as can be seen from Figs. 10(a), 11(a), and 12(a). In all three cases, the vertical focusing increases with the straight-section length, as does the k-sensitivity, particularly at the lower values of k. For the 2(18) structure, above the half-integral superperiod resonance at $Q_Z=7$, and for the 3(15) structure, above the integral superperiod resonance at $Q=6$, stable vertical motion is obtained, but there is a marked discontinuity in the curves at the resonance. The same is probably true of the 2(14) structure, but the region above the integral superperiod resonance was not studied in this case. It is in the radial motion that the dissimiliarities occur. See Figs. 10(b), 11(b), and 12(b). Whereas the radial focusing increases with X/Y in the 2(18) case, it decreases in the other two cases, which also show very marked differences in form. The reasons for these differences are not yet understood. In all three cases the k-sensitivity increases with X/Y towards the larger values of k and as the integral or half-integral resonances are approached, but the 2(14) case shows an extraordinary reversal of the sign of the k-sensitivity at intermediate k-values. In the 2(18) case, it is clear that between $X/Y=\frac{1}{4}$ and $X/Y=\frac{2}{5}$, some new effect has become predominant, and further increases in the straight-section length produce a very rapid decrease in radial focusing and a similar increase in k-sensitivity. In Figs. 10(c), 11(c), and 12(c) these effects are, of course, combined.

It may be concluded from these results that, considered from the standpoint of the existence of stable orbits, it should be possible, in principle, to introduce straight sections of the type described into radial-sector magnets, but there is a limit to the length of the straight section that is permissible. The indications are that a higher basic periodicity is more favorable but, even in the $M=2(18)$ case, the straight sections

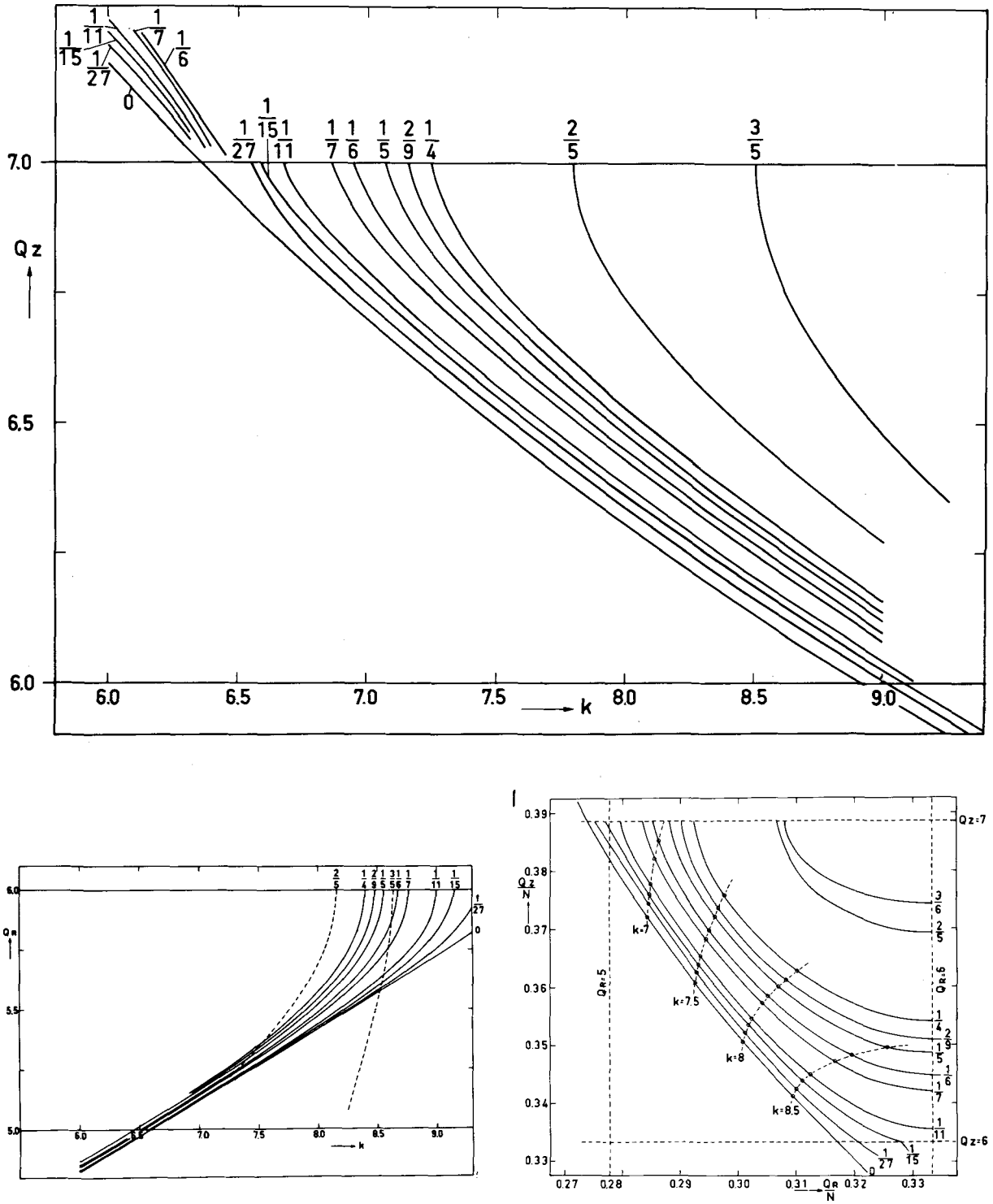

Fig. 10 Linear betatron oscillation frequencies for hard-edge zero-field straight sections: Basic period $N=18$; Superperiod $M=2$. (a) Q_Z vs k. (b) Q_R vs k. (c) Q_Z/N vs Q_R/N. The fractions indicate the superperiodicity ratio X/Y.

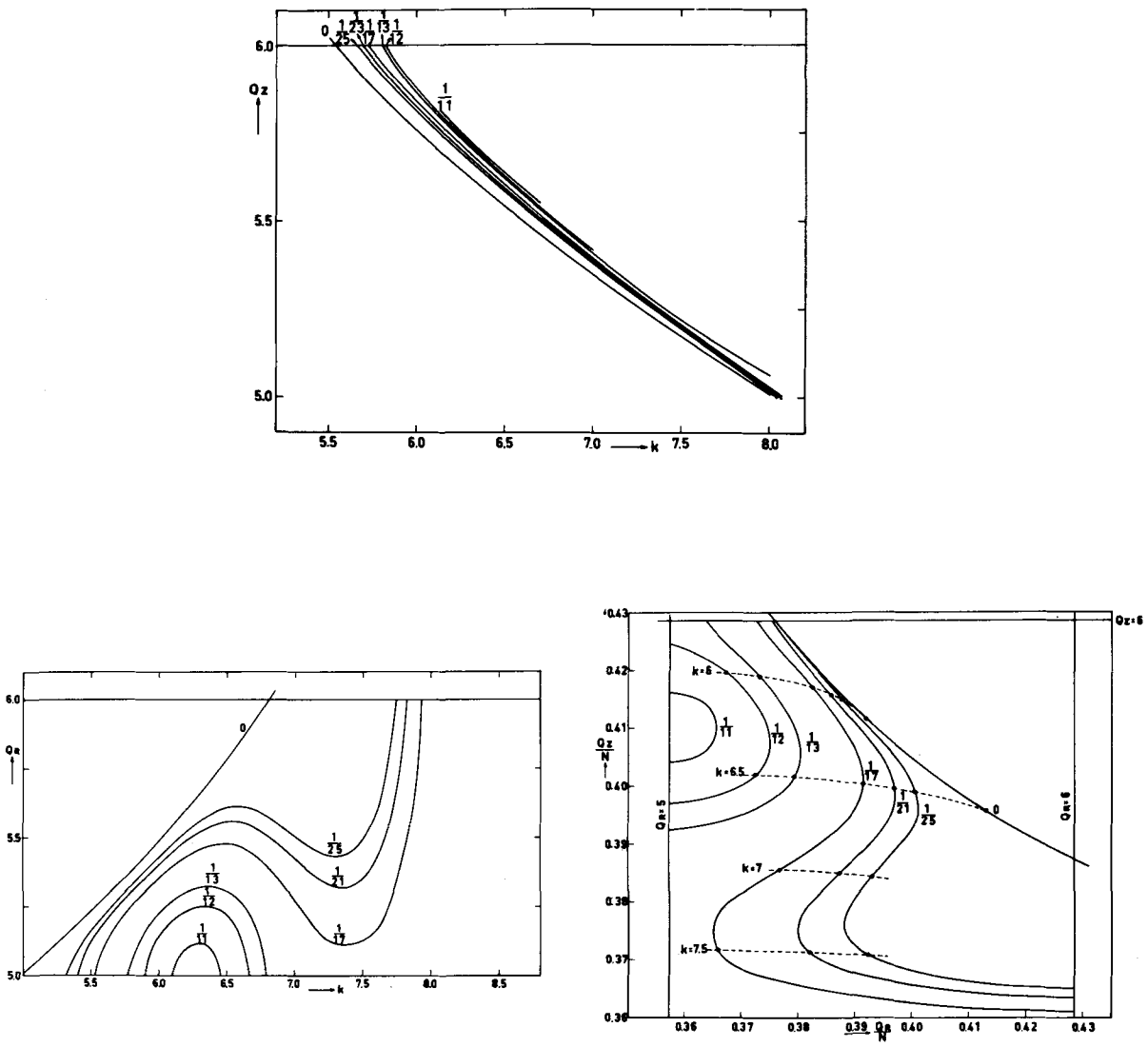

Fig. 11 Similar to Fig. 10, but with $N=14$, $M=2$.

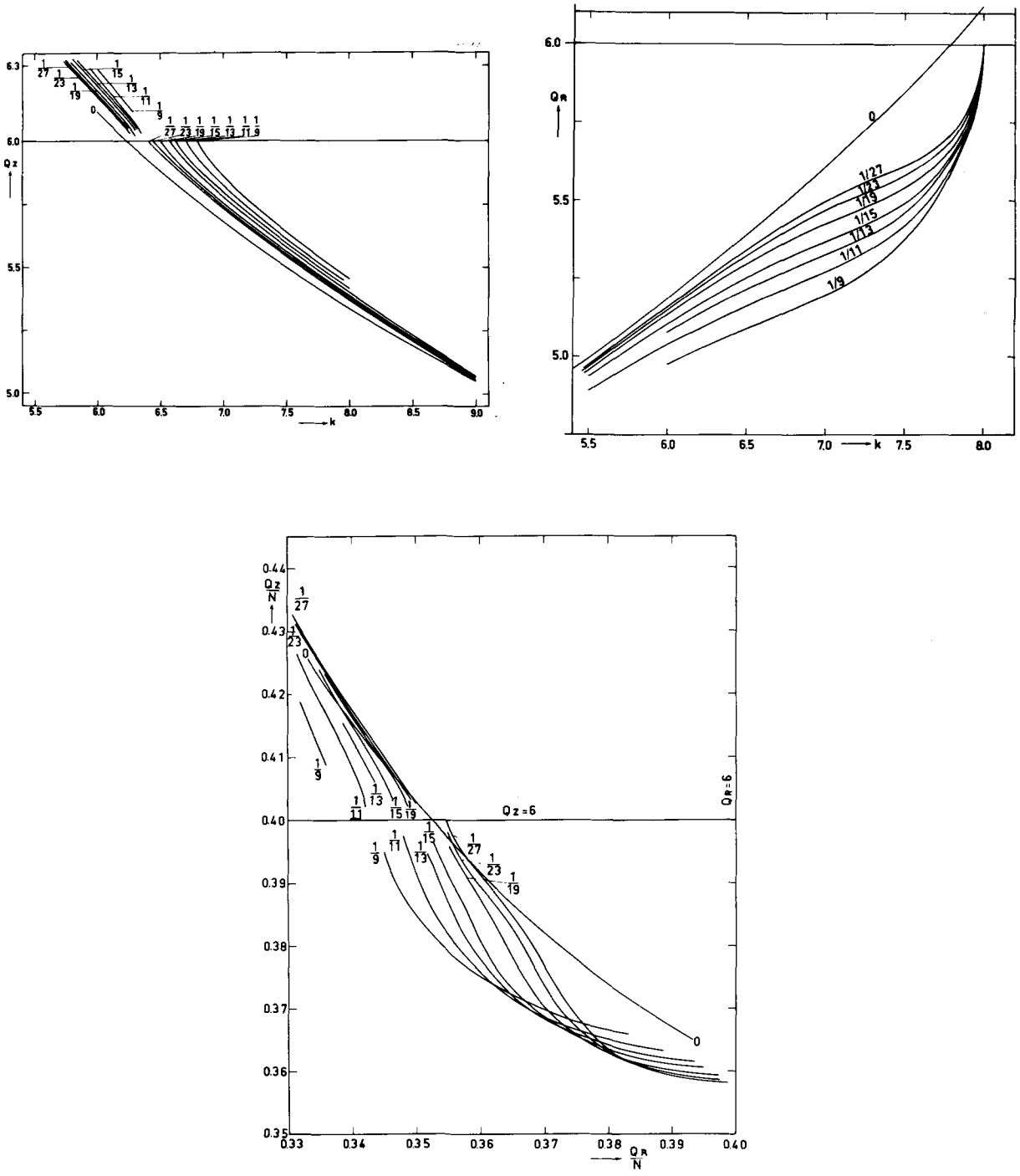

Fig. 12 Similar to Fig. 10 but with $N=15$, $M=3$.

are not very long and the "k-sensitivity" rapidly becomes uncomfortably large. Even in the case $M=2(18)$, $X/Y=\frac{3}{5}$, which has the largest straight section studied, a machine with a maximum orbit circumference of 18 meters would have four straight sections 30 cm wide at the corresponding radius; and although these could accommodate rf cavities, they would be uncomfortably short for most experimental purposes.

It is true that the hard-edged type of flutter function used for these computations may be thought to be a somewhat severe representation of realizable superperiod fields, and that the conclusions may accordingly be pessimistic. Unfortunately, this is not borne out by the admittedly limited results of computations with modified superperiod flutters, which are summarized in subsection E.

It is, of course, necessary to examine also the effect of superperiods on the nonlinear radial and vertical stability limits, and some results have been obtained for a limited number of structures. These are shown in subsection C.

C. Nonlinear Motion

The method of fixed-point searches, described in section 3C, was applied to the superperiod structures also, taking into account the fact that in this case *two* sets of resonances are involved, one pertaining to the superperiod structure and the other to the basic period structure. Tables of rational fractions were again used to predict the order of the resonances that would be encountered as the nonlinear Q_R moved away from its initial, linear value.

As an illustration, the linear Q_R/N in a particular case [$M=3(15)$, $X/Y=1/27$] has the value 0.3988. As the amplitude increases, the motion rapidly becomes nonlinear and passes through the 18th and 13th-order basic-period resonances and the 10th and 9th-order superperiod resonances, before becoming unstable on the 8th-order superperiod resonance. The corresponding rational fractions and their quotients are shown in Table 3.

TABLE 3

Q_R	Q_R/N	*Superperiod resonance* Q_R/M	*Basic period resonance* Q_R/N	*Shift of nonlinear* Q_R
6.0000	0.4000	1	2/5	
5.8333	0.3889		7/18	
5.7692	0.3846		5/13	
5.7000	0.3800	9/10		
5.6667	0.3778	8/9		
5.6250	0.3750	7/8	3/8	←

In other cases, the betatron frequency is observed to traverse a number of internal superperiod resonances before becoming unstable on a higher-order basic period resonance.

Complete fixed-point determinations of the limiting separatrices were made in the cases listed in Table 4. The fixed-point curves for one set of cases [$M=2(18)$] are given in Fig. 13.

If the radial stability limits S_R are compared with the values S_{R0} already found for the corresponding sinusoidal fields without straight sections, it is apparent that the introduction of straight sections very rapidly reduces the size of the stable region, and that this effect is more pronounced the smaller the basic periodicity N. With $M=2(18)$, however, and $x/y=\frac{2}{5}$ (corresponding to a straight-section length of about 7 percent of the orbit radius), the radial stability limit is still large enough for practical purposes.

The form of the fixed-point curves is essentially similar to that of the corresponding structures without superperiods, except for the existence of a much larger number of resonances. When the superperiodicity is weak (small values of X/Y), several internal resonances, both superperiod and basic period, may be traversed before the limiting separatrix is reached, whereas, if the superperiodicity is strong, the separatrix is reached at the nearest superperiod resonance or after traversing only one such resonance if this is near the linear Q_R/N.

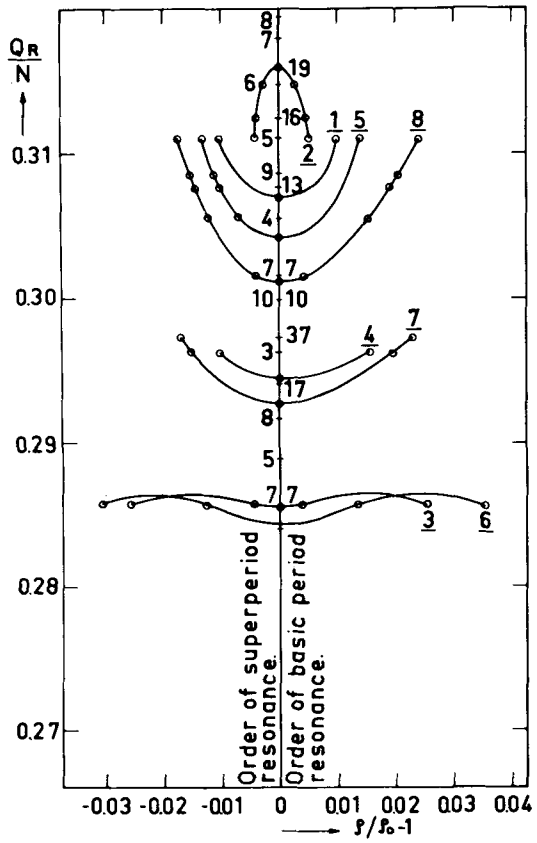

Fig. 13 Fixed point curves for $M=2(18)$:

Curve No.	X/Y	k
1	1/5	8
2	2/5	8
3	1/7	7
4	1/7	7.5
5	1/7	8
6	1/27	7
7	1/27	7.5
8	1/27	8

TABLE 4

Radial Stability Limits for Sinusoidal Structures with Superperiods

Periodicity: $M=2$ $N=14$

Superperiodicity strength $\frac{X}{Y}$	Field index k	Order of limiting separatrix	S_R percent	S_{R0} percent
1/5	8	5	2.04	6.79
2/5	8	5	0.98	6.79
1/7	7	7	5.11	7.03
1/7	7.5	3	3.34	
1/7	8	5	2.73	6.79
1/27	7	7	6.68	7.03
1/27	7.5	37	6.15	
1/27	8	5	4.56	6.79

Periodicity: $M=2$ $N=14$

$\frac{X}{Y}$	k	Order	S_R percent	S_{R0} percent
1/12	6	11	0.39	5.28
1/12	6.5	3	0.43	5.22
1/25	6	3	1.73	5.28
1/25	6.5	5	2.30	5.22
1/25	7.5	7	0.40	5.31

Periodicity: $M=3$ $N=15$

$\frac{X}{Y}$	k	Order	S_R percent	S_{R0} percent
1/27	6.5	4	2.00	2.8
1/27	7.5	7	2.52	4.65
1/27	8	8	1.17	4.42

Because of the close spacing of the superperiod resonances, it is obvious that structures with appreciable superperiodicity must inevitably have much smaller stability limits than the corresponding structures without superperiodicity. The nonlinear axial stability limits for this type of structure were checked in a very limited number of cases, the reason for this being the considerable computer time involved for superperiod fields. It was found that the introduction of straight sections of even moderate length causes a drastic reduction in the axial limits. For the case of an $M=3(15)$ field, with 6 gaps and a field index $k=7.5$, the axial limit S_Z was reduced from 4.6 percent with zero gaps to 0.25 percent with a gap of $X/Y=\frac{1}{9}$.

D. Modified Straight-Section Configurations

The results reported in subsections B and C referred to the particular "hard-edge zero-field" straight-section configuration described in subsection A. To determine whether this configuration had an important influence on the orbits, or whether the main factor was the length of the straight sections, a partial study was made of certain modified configurations.

1. Hard-edge non-zero-field configuration

In this configuration, the field in the straight section is no longer zero, but some fraction, h,

of the maximum field. Two values of h were studied, namely $h=1.0$ and $h=0.4$.

2. Soft-edge non-zero-field configuration

In this configuration, the field in the straight section is not zero (the value $h=0.4$ was used), and, in addition, the field was assumed to have a sinusoidal form in the straight section, as shown in Fig. 14.

3. Hard-edge zero-field unmodified pole angle configuration

In all the above configurations, the azimuthal length of the half-poles on either side of the straight section is the same as that of all the other half-poles in the magnet structure. It follows that, in order to accommodate the straight sections, the angles subtended by all the poles have to be reduced in proportion to the straight-section length, compared with the pole angles of the corresponding structure without superperiods.

Straight sections could also be introduced without changing the pole angles except in the case of the poles adjacent to the straight sections. The resulting configuration is then as shown in Fig. 15.

In order to preserve the condition that the magnetic flux, through the half-poles adjacent to the straight sections, should be equal to that through the normal half-poles (i.e., that the shaded areas in Fig. 15 should be equal), it is necessary to increase the field at the edges of the straight section by a factor b', relative to the maximum field at the center of a normal pole, where b' will increase with the straight-section length. By adding or subtracting an appropriate number of ampere-turns, using a supplementary winding placed around each split pole, one can, with the horizontal return-yoke structure envisaged in all these studies

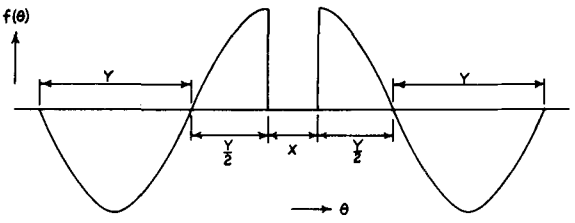

Fig. 14 Soft-edge nonzero-field straight section.

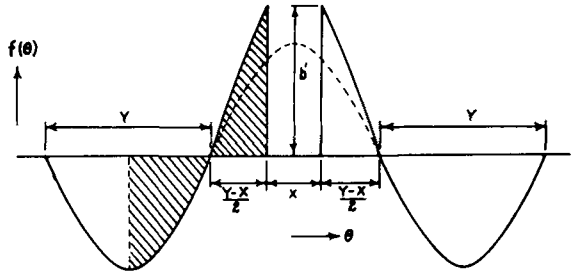

Fig. 15 Hard-edge zero-field unmodified-pole-angle straight section.

(and described in Ref. 4), make the field at the edges of the straight sections either greater, or less than, the value which would satisfy the condition of equal flux. That is, instead of the factor b', one could have a factor b, where the ratio $\beta=b/b'$ may be greater or less than unity. In fact, the use of such supplementary windings was considered as a possible means of tuning the FFAG magnet described in Ref. 4.

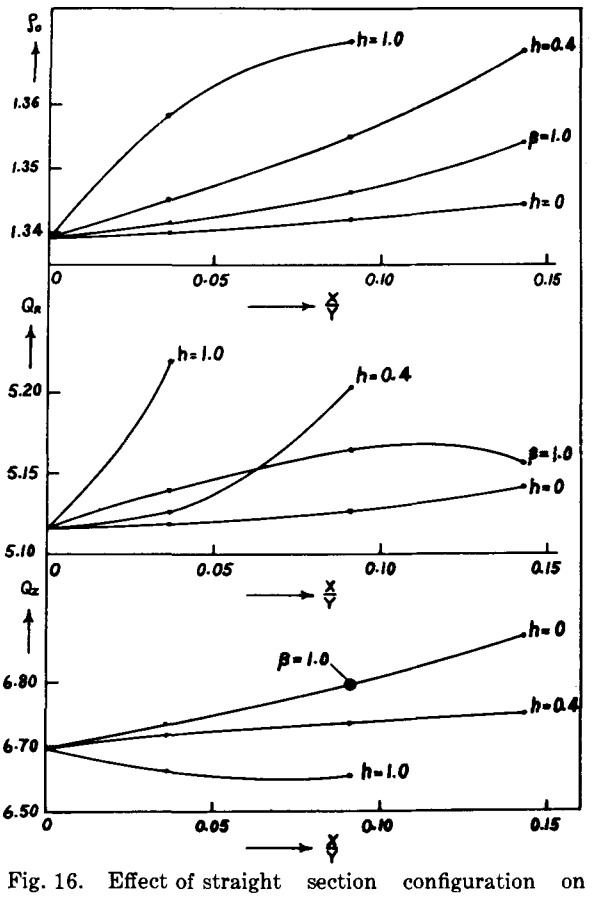

Fig. 16. Effect of straight section configuration on linear motion.

The results obtained with these modified configurations were confined to determinations of the equilibrium-orbit radius and the linear radial and axial betatron frequencies. A fairly typical example of one set of these results, for $M=2(18)$ and $k=7$, is shown in Fig. 16. It is immediately apparent from these results that, contrary to what might have been expected, the precise configuration of the straight section has a more important effect than its size. The results for hard-edge zero-field configurations must therefore be treated with some reserve.

V. FIELDS WITH NON-SINUSOIDAL FLUTTER FUNCTIONS

Only a few fields with nonsinusoidal flutter functions of the particular type,

$$f(\theta) = \sum_{n=1}^{\infty} b_{2n-1} \sin (2_n - 1)\, M\theta \qquad (14)$$

retaining the required features of both symmetry and antisymmetry, have been investigated. For the actual choice of flutter function, we have been guided by measurements performed on the magnet model depicted on Figs. 2, 3 and 4 in Ref. 4. The flutter function, in this model, varies from nearly sinusoidal at smaller radii to nearly trapezoidal at larger radii (Fig. 8, Ref. 4). Calculations show that, whereas the radial betatron-oscillation frequency is almost unaffected by this particular change in flutter, the axial frequency increases as one moves towards the trapezoidal shape (Fig. 9, Ref. 4). The actual harmonic contents of the flutter functions used in these calculations are listed in Table 5, and Table 6 gives the results obtained for the radial and axial stability limits for machines of periodicity $M=14$ and 15 and a field index of $k=6.5$ and 7.0, respectively.

TABLE 5

Harmonic Content of Magnet Model Flutter

	Magnet Model Radius (cm)				
b_i	65	80	95	100	110
b_1	1.000	1.000	1.000	1.000	1.000
b_3	0.006	0.025	0.101	0.178	0.206
b_5	−0.004	−0.004	0.010	0.021	0.030
b_7	0.008	0	0.008	−0.007	−0.019
b_9	0.001	−0.003	0.003	−0.005	−0.019
b_{11}	−0.003	0	0.002	−0.003	−0.006
b_{13}	0.002	0.002	0.004	−0.002	0.004

TABLE 6

Magnet Model Stability Limits

M	k	Model radius (cm)	Q_R/M	Q_Z/M	S_R	S_Z
14	6.5	65	0.4132	0.3962	4.87	2.8
		80	0.4134	0.3981	5.06	2.8
		95	0.4142	0.4083	5.16	2.3
		100	0.4157	0.4234	5.06	1.9
		110	0.4162	0.4309	5.07	1.3
15	7.0	65	0.3742	0.3793	3.90	3.4
		80	0.3743	0.3808	3.80	3.5
		95	0.3749	0.3893	3.89	2.6
		100	0.3756	0.4014	3.90	1.8
		110	0.3760	0.4071	3.80	2.0

Like the radial frequencies, the radial stability limits S_R are practically equal for all flutters. The axial stability limit in the case of $M=15$, $k=7.0$ behaves normally and shows a dip around the $Q_Z/M=\frac{2}{5}=0.4$ resonance, whereas the case of $M=14$, $k=6.5$ shows an inexplicable anomalous behavior in this respect.

It ought, perhaps, to be remembered that the calculations reported here are performed with a digital computer programme which utilizes the scaling property of the magnetic field, a feature which clearly is not present in the magnet model. The results should, therefore, be treated with some reserve. They are only correct for the model field under the provision that the flutter function does not vary appreciably over the range covered by the radial oscillations of the particles.

VI. RADIATION LOSS

In a high-current electron accelerator, as contemplated in the 100-Mev region, the radiated energy loss will become an important design factor, of which it is consequently desirable to perform an accurate calculation. For this we have used the classical formula

$$\frac{dW}{dt} = \frac{\mu_0 q^2}{6\pi c}\gamma^4 v^4 K^2 \qquad (15)$$

valid for a single particle. In this expression, μ_0 is the permeability of free space, c the velocity of light, $\gamma=(1-v^2/c^2)^{-\frac{1}{2}}$, v being the particle velocity, and K the curvature of the orbit at the point under consideration. For a

median-plane orbit, the curvature is immediately given by the particle energy and the field (1). By introducing the scale factor (2), (3) and altering the independent variable from time t to angle θ, one arrives at the formula

$$\frac{dW}{d\theta} = \frac{\mu_0 q^2 c^2}{6\pi S}\gamma(\gamma^2-1)^{3/2}\rho^{2k+1}(1-p_\rho^2)^{-1/2}f(\theta)^2 \quad (16)$$

which may be integrated simultaneously with the orbital equations based on the Hamiltonian (7).

$$C = 0.01533\frac{\gamma}{r_0}(\gamma^2-1)^{3/2} \cdot \sqrt[k+1]{\frac{B_0 r_0}{3\sqrt{\gamma^2-1}}}\,38309^{-\frac{3k+2}{2(k+1)}} \quad (17)$$

where γ is the total- to rest-energy ratio for the particles considered.

It is interesting to compare the computed losses with the loss $\epsilon_0 = 2.96$ ev/turn pertaining to a 100-Mev electron rotating on a circular orbit of radius 3 meter. One finds, in agreement with the results of G. Parzen[7], that the radiation factor $F = \epsilon/\epsilon_0$ rises sharply with increasing period number M, as demonstrated by the example for $k = 8$ shown in Fig. 18. The reason for this increased loss is, of course, the

In Fig. 17 are given curves showing the energy ϵ in electron volts, radiated per turn from a single 100-Mev electron moving on its equilibrium orbit in azimuthally sinusoidal fields defined by $r_0 = 3$ meter, $B_0 = 1$ Wb/m^2 in Eq. (1) and their parameters M, k. It is seen how the energy loss rises with increasing M and decreasing k. The results in Fig. 17 may be converted to fields defined by any other values of r_0 and B_0 and particles of any other type or energy by multiplying the loss read off the figure by the factor

equilibrium-orbit scallop, which results in a larger mean curvature along the orbit than that of the comparable circle.

As demonstrated in section IV, the period number M should be chosen as large as possible if straight sections are to be introduced in the structure with a minimum loss of phase stability. Taking also the radiation losses rising with M into account, one obviously has to reach a compromise on the appropriate choice of M.

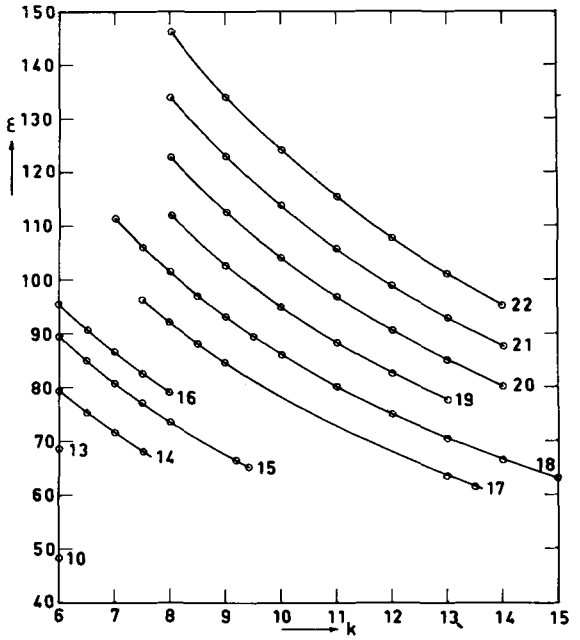

Fig. 17 Radiation loss for electrons on scalloped orbits. Radiation loss ϵ in ev/turn for periodicities $M = 13$ to 22. Electron energy 100 Mev. Orbit radius 3 m.

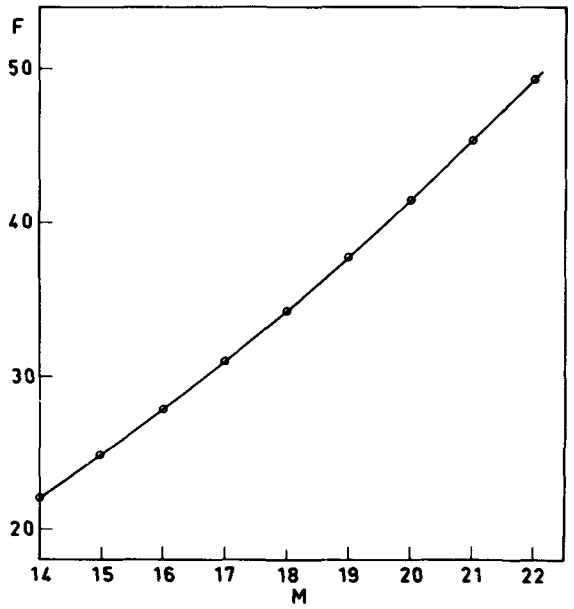

Fig. 18 Radiation factor for electrons on scalloped orbits. Radiation factor $F = \epsilon/\epsilon_0$ for $k = 8$. Electron energy 100 Mev. Orbit radius 3 m.

VII. SUMMARY AND CONCLUSIONS

Digital computation methods have been developed and applied to a comprehensive study of orbits in Two-Way Scaling FFAG Synchrotrons. The computations have so far been confined to magnets of relatively low periodicity and field index, such as would be appropriate to electron accelerators in the energy range up to about 100 Mev, but the methods and computer programmes could be applied equally well to larger proton accelerators with higher periodicity and field index.

The main emphasis has been on machines with sinusoidal field flutter functions and without superperiods, but a preliminary study of the effect of straight sections of a particular idealized form has been made. The calculations include linear betatron-oscillation frequencies, nonlinear radial and axial stability limits and radiation loss.

For sinusoidal fields without superperiods, it is shown that the radial stability limits can be made large enough for practical purposes, provided that the linear radial betatron frequency is not too close to the third-order resonance, and that much larger stability limits can be obtained, together with pseudo-linear radial oscillations, up to very large amplitudes by a proper choice of the parameters M and k. The axial stability limits are generally comparable with the radial, unless the working point lies near the third-order axial resonance or an excitable third-order coupling resonance, in which case the axial limit is considerably reduced.

For machines with approximately the same linear radial betatron frequency, the radial stability limit decreases with increasing periodicity. There is some indication that the same tendency applies to the axial stability limits. Thus, if it is desired to achieve the maximum possible radial and axial stability limits, the lower values of magnet periodicity are preferable, subject to the restriction that the operating point should be correctly situated relative to the third-order and sum resonances. This also gives the lowest radiation losses.

On the other hand, the results obtained for sinusoidal flutters with superperiods indicate that the stability limits are appreciably reduced by the superperiodicity, and that this effect is more marked with the lower values of basic periodicity. For the case of magnets with straight sections, the operating point must be much more carefully chosen to avoid being too close to the more closely spaced superperiod resonances, and this consideration, together with the great increase of k-sensitivity with superperiodicity, indicates that the problem of magnetic-field tolerances will be made increasingly difficult by the insertion of straight sections, even of moderate length. Indeed, it seems possible to insert straight sections long enough to accommodate accelerating cavities, but the longer straight sections, which would be desirable for a pulsed inflector or for experimental purposes, do not seem practicable.

It must be concluded from this that a radial-sector FFAG accelerator is not a particularly convenient device for the study of beam-stacking processes, as such, although it may be of interest for other purposes. If, furthermore, it is desired to stack appreciable currents of electrons at energies in the 100-Mev region, for instance, to study relativistic space-charge effects, the large radiation factor, which increases rapidly with magnet periodicity, creates serious problems in connection with radiation anti-damping and with the design of an rf system to replace the radiative energy loss.

It is for these reasons, and in view of the immediate interest in the question of stacking efficiency, as such, in relation to possible applications to high-energy accelerators, that the Accelerator Research Division at CERN has decided not to proceed with the construction of the 100-Mev two-way FFAG electron synchrotron described in Ref. 4, but is constructing instead a 2-Mev electron storage ring.

VIII. ACKNOWLEDGEMENTS

For the construction of the computer programmes, we owe much to the help and suggestions from the CERN digital computer staff, in particular N. H. Lipps, G. Erskine, D. Lake, D. Ball and F. Louis. In our own group, we are indebted to P. T. Kirstein, who has given invaluable help on computational methods and programming. Finally we wish to express our

thanks to M. Hanney, Y. Jayet, P. Corp, D. Fortune and S. Burgeois for their assistance in the routine handling of data and results, and running of the programmes.

REFERENCES

1. *The MURA Two-Way Electron Accelerator*, CERN Symposium 1959, page 71.
2. TIHIRO OHKAWA, *On the Two-Beam FFAG Accelerator*, MURA-318, July 5, 1957.
3. L. J. LASLETT and K. R. SYMON, *Particle Orbits in Fixed Field Alternating Gradient Accelerators*, CERN Symposium 1956, Vol. I, page 279.
4. M. BARBIER et al., *Studies of an Experimental Beam-Stacking Electron Accelerator*, CERN Symposium 1959, page 100.
5. NILS VOGT-NILSEN, *The Magnetic Field and Orbital Equations for a Fixed Field Two-Way Scaling Accelerator*, CERN 60-15.
6. R. HAGEDORN, M. G. N. HINE and A. SCHOCH, *Non-Linear Orbit Problems in Synchrotrons*, CERN Symposium 1956, Vol. I, page 237.
7. G. PARZEN, *The Radiation Energy Loss in a Fixed Field Accelerator*, MURA-376, Nov. 14, 1957.

DISCUSSION

K. R. SYMON: When you introduced the straight sections, did you readjust the parameters so that the Q-values with the straight sections are in a reasonable part of the working-point diagram?

N. VOGT-NILSEN: No, but we tried to cover so many cases that we could choose an initial point such that, with the straight sections, we could end up at a reasonable place in the diagram.